RESEARCH ARTICLE

WILEY

Coupling relationship between glucose and oxygen metabolisms to differentiate preclinical Alzheimer's disease and normal individuals

Changchang Ding[1] | Wenying Du[2] | Qi Zhang[1] | Luyao Wang[3] | Ying Han[2,4,5,6] | Jiehui Jiang[1]

[1]Key Laboratory of Specialty Fiber Optics and Optical Access Networks, Joint International Research Laboratory of Specialty Fiber Optics and Advanced Communication, School of Communication and Information Engineering, Shanghai University, Shanghai, China

[2]Department of Neurology, Xuanwu Hospital of Capital Medical University, Beijing, China

[3]School of Mechatronical Engineering, Beijing Institute of Technology, Beijing, China

[4]Center of Alzheimer's Disease, Beijing Institute for Brain Disorders, Beijing, China

[5]National Clinical Research Center for Geriatric Disorders, Beijing, China

[6]Biomedical Engineering Institute, Hainan University, Haikou, China

Correspondence
Jiehui Jiang, School of Communication and Information Engineering, Shanghai University, 99 Shangda Road, Shanghai 200444, China.
Email: jiangjiehui@shu.edu.cn

Abstract

The discovery of preclinical Alzheimer's disease (preAD) provides a wide time window for the early intervention of AD. The coupling relationships between glucose and oxygen metabolisms from hybrid PET/MRI can provide complementary information on the brain's physiological state for preAD. In this study, we purpose to explore the change of coupling relationship among 27 normal controls (NCs), 20 preADs, and 15 cognitive impairments (CIs). For each subject, we calculated the Spearman partial correlation between the fractional amplitude of low-frequency fluctuations (fALFF) and the regional homogeneity (ReHo) from functional image (fMRI), and the standard uptake value ratio (SUVR) from [18F] fluorodeoxyglucose positron emission tomography (^{18}F-FDG PET), in the whole-brain and default mode network (DMN) as a novel potential biomarker. The diagnostic performance of this biomarker was evaluated by the receiver operating characteristic analysis. Significant Spearman correlations between the FDG SUVR and the fALFF/ReHo were found in 98% of subjects. For the DMN-based biomarker, there was a significant decreasing trend for the preAD and CI groups compared to the NC group, whereas no significant difference in preAD based on whole-brain. The correlation ρ value for the FDG SUVR/ReHo showed the highest area under curve of the preAD classification (0.787). The results imply the coupling relationship changed during the preAD stage in the DMN area.

KEYWORDS
default mode network, functional magnetic resonance imaging, position emission tomography, preclinical Alzheimer's disease

1 | INTRODUCTION

Alzheimer's disease (AD) is a neurodegenerative disease characterized by progressive cognitive decline. Amyloid-β (Aβ) and tau

accumulation occurs in the forms of amyloid plaques and neurofibrillary tangles in the brain of an AD patient, which is accompanied by neural degeneration and loss (Chételat, 2013; Duan et al., 2016; Wang et al., 2020). The brain alternations due to AD may precede memory impairment, which can be detected by neuroimaging methods (Balsis et al., 2018; Habib et al., 2017; Sun et al., 2016). With the progress of AD research, the focus has gradually shifted to the early stage of the disease, for example, preclinical AD (preAD), which refers to the stage without cognitive impairment (CI) but with abnormal AD biomarkers (Aβ+). The discovery of preAD can provide a wide time window for the early intervention of AD (Jessen et al., 2020; Molinuevo et al., 2017; Palaniyappan & Liddle, 2014; Wang et al., 2020).

Glucose and oxygen metabolisms are closely related, and both are concerned with the nerve activity in the resting state (Aiello et al., 2015; Baron et al., 1984; Dong et al., 2021; Jueptner & Weiller, 1995). These two types of metabolisms are relatively stable in a normal human brain. However, the coupling relationship between the two metabolisms may be damaged by neurodegenerative disorders, such as AD (Aiello et al., 2015; Marchitelli et al., 2018). To explore the above changes, scholars have used neuroimaging techniques to present the two metabolisms. Some examples are [18F] fluorodeoxyglucose positron emission tomography (^{18}F-FDG PET), which presents glucose metabolism, and resting-state functional magnetic resonance imaging (rs-fMRI), which represents oxygen metabolism. In addition, extracted semi-quantitative indicators, including standardized uptake value ratio (SUVR) from FDG PET, fractional amplitude of low-frequency fluctuations (fALFF), and regional homogeneity (ReHo) from fMRI and the calculated the correlation ρ value between the FDG SUVR and the fALFF/ReHo present the real-time coupling relationship in vivo.

Consequently, hybrid FDG PET/MRI scans have been used to explore the variation in the correlation between the glucose and oxygen metabolisms in the resting state in normal control (NC) and AD subjects by calculating the correlation ρ value between the FDG SUVR and the fALFF/ReHo. For instance, Aiello et al. found a significant and stable correlation between the FDG SUVR and the fALFF/ReHo in the global brains of NC subjects, which indicated that the correlation ρ value is useful to represent the coupling relationship (Aiello et al., 2015). Based on this, Marchitelli et al. further determined a significant coupling reduction in patients with CI at the entire brain level (Marchitelli et al., 2018). However, whether the coupling relationship changes in preAD needs further exploration.

Therefore, in the present study, first, we aimed to explore whether the correlation ρ value between the FDG SUVR/fALFF and the SUVR/ReHo in the preAD stage varies compared to that in NC subjects. Because we proposed that the changes may be small and local, we compared the ρ values at both the global brain and default mode network (DMN) levels. DMN is well known as an important brain region for AD disease spectrum. Second, we aimed to explore the diagnosis performance of the correlation ρ values as biomarker among NC, preAD, and CI groups.

2 | MATERIALS AND METHODS

2.1 | Subjects

In this study, we examined 62 right-handed and Mandarin-speaking subjects with ages ranging 50–79 years, comprising 27 NC subjects, 20 preADs, and 15 CI patients. The data were obtained from the Sino Longitudinal Study on Cognitive Decline (SILCODE) project (Li, Wang, Su, Hu, & Han, 2019) (ClinicalTrials.gov Identifier #NCT03370744). The entire group of the subjects underwent routine clinical and standard laboratory assessments, including a neurological examination, neuropsychological evaluation, brain simultaneous resting-state FDG-PET, and fMRI acquisition. The Aβ values of all the NC and preAD subjects and a part of the CI subjects ($N = 7$) were selected by ^{18}F-florbetapir (^{18}F-AV45) PET. Moreover, all the subjects were required to obtain written informed consent prior to enrollment.

NC was defined as the subjects with normal performance in neuropsychological tests and negative amyloid burden (Aβ-) in ^{18}F-AV45 PET scans. PreAD was defined with the criteria based on the National Institute on Aging-Alzheimer's Association (NIA-AA; Sperling et al., 2011) and International Working Group-2 guidelines (Dubois et al., 2014) as positive amyloid burden in AV45-PET relative to the population with normal cognitive level. The CI group comprised subjects with amnestic mild CI (aMCI) or AD dementia. The inclusion criteria for aMCI were based on the actuarial neuropsychological method proposed by Jak and Bondi (Bondi et al., 2014). The inclusion of AD dementia was based on the Diagnostic and Statistical Manual of Mental Disorders Fifth Edition and the diagnostic guidelines for dementia due to AD established by NIA-AA workgroups (McKhann et al., 2011). The detailed definitions of preAD and CI are provided in the Supporting Information.

All the subjects underwent neurological examination, which comprised the Chinese version of the mini-mental state examination (MMSE), basic version of Montreal cognitive assessment (MoCA-B), Hamilton depression rating scale (HAMD), Hamilton anxiety rating scale (HAMA), subjective cognitive decline (SCD-9), shape trail test A (STT-A), shape trail test B (STT-B), animal fluency test (AFT), Boston naming test (BNT), geriatric depression scale (GDS), long-term delayed recall (N5), and recognition (N7). The exclusion criteria were current major psychiatric diagnoses (e.g., severe depression or anxiety), other neurological conditions or those which can cause cognitive decline (e.g., Parkinson's disease, encephalitis, or thyroid dysfunction) instead of AD spectrum disorders, and the inability to complete the study protocol or presence of contraindications for MRI. Furthermore, the subjects with an MMSE score of less than 27 in the normal cognitive group and more than 26 in the CI group were excluded (Folstein, Folstein, & McHugh, 1975).

2.2 | Image acquisition

An integrated 3.0 T TOF PET/MR (SIGNA PET/MR, GE Healthcare, Milwaukee, Wisconsin) at the Xuanwu Hospital of Capital Medical University was used to simultaneously acquire the PET and MRI data.

The parameters for the three-dimensional (3D) T1-weighted MRI images acquired by a spoiled gradient-recalled sequence were as follows: repetition time (TR) = 6.9 ms, echo time (TE) = 2.98 ms, inversion time (TI) = 450 ms, flip angle = 12°, voxel size = $1 \times 1 \times 1$ mm^3, field of view (FOV) = 256×256 mm^2, matrix size = 256×256, slice thickness = 1 mm, and slice number = 192. Resting-state fMRI was obtained with a single-shot gradient-echo planar imaging sequence with the following parameters: TR = 2000 ms, TE = 30 ms, flip angle = 90°, voxel size = $3.5 \times 3.5 \times 4$ mm^3, FOV = 224×224 mm^2, matrix size = 64×64, slice thickness = 4.0 mm, slice number = 28, and slice order = interleaved.

In this study, all the subjects underwent ^{18}F-FDG PET/MRI scans. ^{18}F-AV45 PET was performed to assess the cortical Aβ burden for all the NC and preAD subjects and a part of the CI patients ($N = 7$). The interval between the recording of FDG-PET and AV45-PET was more than 3 days to eliminate the influence of the first tracer. For FDG-PET, each subject was instructed to fast for a minimum of 6 hr, and a 35-min dynamic scan was acquired approximately 40 min after an intravenous injection of 3.7 MBq/kg of ^{18}F-FDG. For Aβ-PET, a 35-min dynamic scan was acquired approximately 40 min after an intravenous injection of 7–10 mCi ^{18}F-AV45. The PET data were acquired in the 3D acquisition mode and using a time-of-flight ordered subset expectation maximization algorithm with the following parameters: eight iterations, FOV = 350×350 mm^2, 32 subsets matrix = 192×192, and full width at half maximum (FWHM) = 3.

2.3 | Structural MRI processing

The 3D high-resolution T1-weighted images were captured by a standard voxel-based morphometric analysis using a computational anatomy toolbox (CAT12, http://dbm.neuro.uni-jena.de/cat/) on a MATLAB 2016b platform. For each T1 image preprocessing, first, image registration was performed, followed by segmentation into probabilistic gray matter (GM), white matter (WM), and cerebrospinal fluid (CSF). Each GM image was normalized to the Montreal Neurological Institute (MNI) space by diffeomorphic anatomical registration via exponentiated lie algebra, and finally smoothed using an 8-mm Gaussian-smoothing kernel.

Brain atrophy has been proved to be closely related to the pathology and memory impairment in AD (Gupta, 2020; Pegueroles et al., 2017). In this study, CAT12 was also used to automatically calculate the bilateral hippocampal volume (HPV), bilateral basal forebrain volume (BFV), GM volume (GMV), and total intracranial volume (TIV) as general indicators for comparison with the FDG-PET/fMRI correlation metrics. Briefly, local GM and WM volumes are conserved by modulating the image intensity of each voxel by the Jacobian determinants of the computed deformation fields during the normalization. The anatomical structures of the hippocampus and the bilateral basal forebrain were extracted from normalized and modulated GM maps based on a neuromorphometrics atlas (http://neuromorphometrics.com/). The TIV of each subject was estimated by adding the segmented GM, WM, and CSF volumes. In this study,

GM and DMN binary spatial masks, also based on structural MRI, were used to extract the voxel values from FDG-PET and fMRI images.

2.4 | Resting-state fMRI image preprocessing

Resting-state fMRI images were preprocessed using the Data Processing Assistant for Resting-State fMRI (DPARSF, http://www.rfmri.org/DPARSF) software implemented on the MATLAB 2016b platform.

To minimize the influence of magnetic field inhomogeneity during the initial scanning, the data of the first 10 time points were removed. Slice-timing corrections followed by head motion correction and baseline drift removal were conducted on the remaining 230 time point data to eliminate the impact of different acquisition times. Studies with an estimated maximum head motion larger than 3.0 mm and/or 3.0° were excluded. Multiple linear regression analysis was performed on 24 head movement parameters (12 movement parameters and their first derivatives) and mean time series of WM, CSF, and global brain to remove additional false physiological noise sources. The resulting images were normalized to the MNI standard space using the transformation parameters of the structural image normalized to the MNI standard space with resampling to 3 mm isotropic voxels. Subsequently, they were smoothed by a 4-mm FWHM Gaussian smoothing kernel (Yan et al., 2020).

2.5 | PET image processing

The ^{18}F-FDG PET and ^{18}F-AV45 PET images were preprocessed using a statistical parametric mapping software (SPM12, https://www.fil.ion.ucl.auk/spm/software/spm12/) with MATLAB 2016b.

For ^{18}F-FDG PET, all the PET images were co-registered with T1-weighted 3D MRI images. Partial volume correction (PVC) was applied to the images after registration to minimize the partial volume effects on the PET measurements. PVC for removing the partial volume effect on the PET images was based on the Muller–Gartner algorithm and a three-compartment model (Gonzalez-Escamilla, Lange, Teipel, Buchert, & Grothe, 2017). The PET images after the PVC were spatially normalized to the MNI space using the transformation parameters of T1 MRI image standardization to the MNI space. Finally, the resulting images were smoothed by an 8-mm FWHM Gaussian smoothing kernel. The SUVR of each PET image was calculated with the global brain under the GM mask as the reference area.

For ^{18}F-AV45 PET, in brief, the PET images were registered into structural images and subsequently spatially normalized to the MNI space using the transformation parameters from the spatial standardization of the MRI images. This was followed by smoothing with an 8-mm FWHM Gaussian kernel. The ^{18}F-AV45 PET images were normalized using the cerebellum based on Anatomical Automatic Labeling (AAL) template (area: 91–116) as a reference region to obtain the SUVR. In this study, normal cognitive subjects were classified as

Aβ positive (Aβ [+]) or Aβ negative (Aβ [−]) in relation to a cutoff of 1.18 SUVR in the AV45 PET scans (Chen et al., 2015).

2.6 | Rs-fMRI metrics

The spontaneous activity of the brain is closely related to the cognitive activity in the resting state. In this study, fALFF and ReHo were used based on previous studies (Aiello et al., 2015; Marchitelli et al., 2018).

The fALFF is the ratio of the power in the low-frequency range (0.01–0.1 Hz) and the total power in the entire detectable frequency range of each voxel time process. It quantifies the amplitude of the low-frequency oscillation (LFO) to represent the relative LFO contribution to the entire frequency range (Zou et al., 2008; Zuo et al., 2010). The fALFF can effectively inhibit the energy of the non-physiological brain regions affected by noise and CSF and improve the sensitivity and specificity of spontaneous nerve activity signal detection.

ReHo reflects the spontaneous neural activity in the brain from the perspective of the interconnections between neurons. The theoretical basis is that under certain conditions, the voxels in the brain region and the surrounding voxels have high temporal consistency. In a time series, the similarity between a certain voxel in the brain and its adjacent 27 voxels is calculated, and Kendall's coefficient of harmony (KCC; Zang, Jiang, Lu, He, & Tian, 2004) is obtained. The KCC value is used to represent the consistency of the time series between non-adjacent voxels around the brain area, which indirectly reflects the synchronous consistency of the neuronal activities in local brain regions.

After calculating the fALFF and ReHo maps, each map was normalized to obtain a z-score map by calculating the ratio of the difference between the average value of each voxel and GM voxel to the *SD*. In this study, global and DMN ReHo/fALFF were defined as the GM voxel means under GM and DMN masks, respectively, (Yeo et al., 2011) as conventional metrics for evaluating spontaneous brain activity.

2.7 | FDG-PET/fMRI correlation metrics

Previous findings of CI have weakened the coupling relationship between the glucose metabolism and the functional activity in the entire brain (Aiello et al., 2015; Marchitelli et al., 2018). To evaluate the relationship for preAD, we performed the same operations on ^{18}F-FDG PET and fMRI as in the study of Aiello et al.

After preprocessing and standardizing into the z-score, the FDG SUVR maps, GM probability, and fALFF and ReHo maps were transformed into one-dimensional vectors using a GM or DMN mask. Spearman's rank correlation (ρ) was performed between the one-dimensional vector from two imaging modalities, and the regression of the GM probability value was used to minimize the bias caused

by unnecessary structural atrophy. Therefore, the global or DMN FDG-PET/fMRI correlation was calculated using a GM or DMN mask and the correlation coefficients—global SUVR/fALFF (ρ), global SUVR/ReHo (ρ), DMN SUVR/fALFF (ρ), and DMN SUVR/fALFF (ρ)—defined as a category of PET/fMRI correlation metrics to analyze the changes in preAD and CI stages. To define the high coupling and lower coupling regions, we used the AAL atlas (116 brain regions) to calculate the coupling relationships at the level of brain regions. Spearman correlation coefficient value .3 was chosen as the threshold to discriminate high coupling and low coupling regions (Mukaka, 2012).

2.8 | Statistical analysis

In this study, scalar statistical analysis was conducted using IBM SPSS statistics V25.0, and voxel-based statistical evaluation was performed in Data Processing & Analysis for Brain Imaging (DPABI, http://rfmri.org/dpabi). The statistical significance level was set as *p* < .05.

2.8.1 | Demography and neuropsychology

A chi-squared test was conducted to evaluate the gender effect among the samples, and analysis of variance (ANOVA) was used to evaluate the statistical differences in the age, MMSE, and other neuropsychological scale scores of the three groups (NC, preAD, and CI).

2.8.2 | Spatial distribution difference analysis

To verify the repeatability of the SUVR, fALFF, and ReHo, an independent two-sample *t*-test at whole brain level was performed on the complete individual datasets of the NC and CI groups (NC > CI), and NC and preAD groups (NC > preAD) under regression of the gender, age, and education. In addition, the GM probability map was included as a based-voxel covariate to deal with the variability in the GM density in the different populations due to the effect of the GM atrophy on these comparisons (Xie et al., 2015). Finally, Gaussian random field (GRF) correction (minimum, z > 2.5; voxel level *p* < .01, cluster level *p* < .05) was applied to each t-map obtained by the two-sample *t*-test, followed by the observation of the group differences in the spatial distribution.

2.8.3 | Conventional and FDG-PET/fMRI correlation metrics

To observe the distribution of the FDG-PET/fMRI correlation metrics between the groups, ANOVA was used to compare the HPV, BFV, GMV, and TIV in the structural images. The quantified functional indicators (global fALFF, global ReHo, DMN fALFF, and DMN ReHo) and the FDG-PET/fMRI correlation metrics among the groups were

also employed to explore if these indicators can differentiate between the groups.

2.8.4 | Correlation analysis with Aβ

AD is characterized in the late stages by Aβ plaques and neurofibrillary tangles. To explore if there exists a correlation between the FDG SUVR, fALFF, ReHo, and Aβ SUVR in NC and preAD subjects, the partial Pearson correlation between the global AV45 SUVR, conventional indicators, and FDG-PET/fMRI correlation metrics was calculated using the SPSS software for a statistical significance of $p < .05$. Subsequently, the subjects who underwent AV45-PET in the CI group were added to explore the changes in the correlation caused by CI.

2.8.5 | Classification performance analysis

Receiver operating characteristic (ROC) analysis was performed to explore the diagnostic performance of the conventional indicators and the FDG-PET/fMRI metrics among the three groups. The ROC curve of each indicator was drawn, and the area under the curve (AUC) calculated using the SPSS software was considered statistically significant when $p < .05$. Subsequently, the Youden index was used to determine the optimal threshold of the ROC curve and its corresponding sensitivity and specificity.
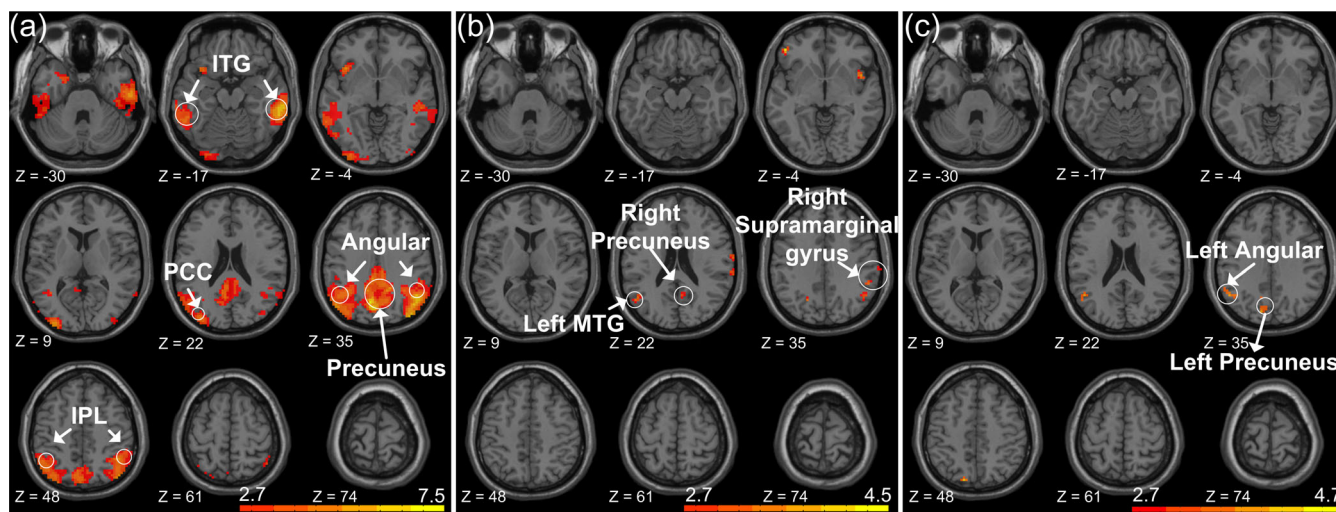
3 | RESULTS

3.1 | Demography and neuropsychology

Based on the chi-square test and the ANOVA analysis, there were no significant difference in the gender, age, and education among the groups. There were significant differences in the MMSE, MoCA-B, SCD-9, STT-A, STT-B, AFT, and BNT scores of the CI and NC groups ($p < .05$), even including the preAD group. In addition, there was a significant difference in the HAMA scale scores only of the preAD and CI groups ($p < .05$). The demographic data and cognitive psychology evaluation of the NC, preAD, and CI groups are summarized in Table 1.

3.2 | Spatial distribution difference analysis

Based on the independent two-sample t-test, compared with the NC group, in the CI group, the areas of significant metabolic decline were mainly distributed in the DMN regions, such as angular gyrus, inferior parietal lobule, precuneus, middle temporal gyrus, inferior temporal gyrus, and posterior cingulate cortex. Moreover, the areas with significant decrease were symmetrical in the spatial distribution (Figure 1a). ReHo and fALFF indexes failed to pass GRF correction. The results of two-sample t-test for ReHo and fALFF were significant (cluster > 30), whereas did not pass the GRF correction. The areas in which the

TABLE 1 Data and cognitive psychology evaluation

Characteristics	NC	preAD	CI
Gender (M/F)	11/16	5/15	5/10
Age (year)	65.07 ± 3.44	67.10 ± 5.50	69.33 ± 10.81
Education	13.30 ± 2.32	12.65 ± 2.63	12.67 ± 3.40
MMSE	29.11 ± 0.88[a]	29.20 ± 0.98[b]	19.20 ± 5.58[a,b]
MoCA-B	26.67 ± 1.70[a]	26.70 ± 1.79[b]	14.33 ± 4.76[a,b]
SCD-9	4.22 ± 2.46[a]	4.40 ± 2.03[b]	6.50 ± 1.66[a,b]
HAMD	2.56 ± 3.06[a]	4.00 ± 3.63	5.87 ± 5.28[a]
HAMA	3.41 ± 3.26	4.25 ± 2.55	6.00 ± 5.05
STT-A	54.93 ± 13.96[a]	57.005 ± 22.21[b]	127.46 ± 65.37[a,b]
STT-B	115.04 ± 19.82[a]	132.77 ± 35.68[b]	289.56 ± 192.47[a,b]
AFT	20.44 ± 4.82[a]	19.65 ± 4.36[b]	9.73 ± 3.75[a,b]
BNT	26.07 ± 2.49[a]	25.80 ± 2.69[b]	17.40 ± 5.25[a,b]
GDS	1.93 ± 2.65	2.60 ± 2.13	2.64 ± 2.02
N5	8.23 ± 2.37[a]	7.80 ± 1.69[b]	0.86 ± 1.55[a,b]
N7	22.55 ± 1.37[a]	22.35 ± 1.88[b]	15.14 ± 3.02[a,b]

Note: Data are mean ± *SD*.
Abbreviations: AFT, Animal Fluency Test; BNT, Boston Naming Test; CI, cognitive impairment; GDS, Geriatric Depression Scale; HAMD, Hamilton Depression Rating Scale; HAMA, Hamilton Anxiety Rating Scale; M/F, Male/Female; MMSE, Mini Mental Status Examination; MoCA-B, Basic Version of Montreal Cognitive Assessment; NC, normal control; preAD, preclinical Alzheimer's disease; SCD-9, Subjective Cognitive Decline; STT-A, Shape Trail Test A; STT-B, Shape Trail Test B.
[a]$p < .05$ NC versus CI.
[b]$p < .05$ preAD versus CI.

FIGURE 1 Voxel-based spatial distribution differences among groups. Figure shows Montreal Neurological Institute (MNI) surface rendering with both transverse views, overlaid with results from between-group statistical analysis using NC > CI contrast. Default mode network (DMN) is main area where CI decreases glucose metabolism and functional activities. Area of metabolic decline (FDG SUVR) in CI group compared with NC group (a), expressed as z-scores ($p < .05$) and are corrected for Gaussian random field (GRF) correction method (voxel level $p < .01$, cluster level $p < .05$). The results of ReHo (b) and fALFF (c) were significant (cluster >30) without GRF correction. CI, cognitive impairment; FDG, fluorodeoxyglucose; fALFF, fractional amplitude of low-frequency fluctuations; IPL, inferior parietal lobule; ITG, inferior temporal gyrus; MTG, middle temporal gyrus; NC, normal control; PCC, posterior cingulate cortex; ReHo, regional homogeneity; SUVR, standardized uptake value ratio

ReHo of the CI group decreased compared to that of the NC group were mainly distributed in the right supramarginal, left middle temporal gyrus, and angular gyrus (Figure 1b), consistent with previous research. In addition, the fALFF values of the CI group decreased in the left angular gyrus and precuneus (Figure 1c). It is worth noting that we have also performed two sample t-tests based on the voxels of the NC and preAD groups for the SUVR, ReHo, and fALFF, respectively; however, no clear voxel clusters were found after GRF correction.

3.3 | Conventional and FDG-PET/fMRI correlation metrics

There was no statistical difference between the preAD and NC groups in terms of either the conventional structural or functional indicators. Among the structural indicators, there were significant differences in the HPV, left BFV, and GMV of the CI group and the other groups ($p < .05$). Regarding the functional indicators, there were significant differences in the DMN SUVR, DMN fALFF, and DMN ReHo of the CI group and the other groups. Moreover, there was a significant difference in the global SUVR of the CI and NC groups. The details of the results based on the conventional metrics are summarized in Table S1 and shown in Figure S1.

Regarding the subject FDG-PET/fMRI correlations, there was a strong correlation between the FDG SUVR/fMRI at both the global brain and DMN levels. Specifically, the global SUVR/fALFF (ρ) (NC: −0.06–0.45, preAD: −0.35–0.31, CI: 0–0.59) and the global SUVR/ReHo (ρ) (NC: 0.21–0.57, preAD: 0.07–0.51, CI: −0.05–0.44) ranged from weak to strong. ANOVA showed that the global SUVR/fALFF (ρ)

and the SUVR/ReHo (ρ) of the CI group were lower compared to those of the NC group ($p = .041$ and $p < .001$, respectively). In comparison, in the preAD group, both correlation metrics did not change significantly ($p > .05$) (Figure 2a,b). The DMN SUVR/fALFF (ρ) was found to be statistically significant in 95.16% of the subjects (NC: −0.06–0.46, preAD: 0–0.59, CI: −0.17–0.29) and DMN SUVR/ReHo (ρ) (NC: 0.21–0.55, preAD: 0.09–0.49, CI: −0.15–0.41) in all the subjects ($p < .05$). Compared with the global brain-based FDG-PET/fMRI correlation metric, preAD caused the DMN SUVR/fALFF (ρ) ($p < .024$) and the DMN SUVR/ReHo (ρ) ($p = .002$) to significantly decrease (Figure 2c,d).

Figure 3 showed results on high coupling and low coupling regions. The high coupling regions of SUVR/fALFF (ρ) in NC and preAD groups were mainly distributed in the bilateral rectus, bilateral posterior cingulate gyrus, bilateral lingual, bilateral precuneus, bilateral thalamus, and cerebellum. The low coupling regions were mainly distributed in the bilateral precuneus, bilateral lingual, and right parahippocampal (Figure 3a). For SUVR/ReHo (ρ), the high coupling regions in NC and preAD groups were mainly distributed in the frontal lobe, bilateral precuneus, bilateral calcarine, bilateral lingual, bilateral posterior cingulate gyrus, and bilateral middle temporal gyrus. The low coupling regions were mainly distributed in the bilateral middle temporal gyrus and right inferior temporal gyrus (Figure 3b). In summary, the results showed that most of the high coupling regions were distributed in the DMN region.

3.4 | Correlation analysis with Aβ

Pearson partial correlation analysis demonstrated that the AV45 SUVR was significantly correlated with the global SUVR/ReHo
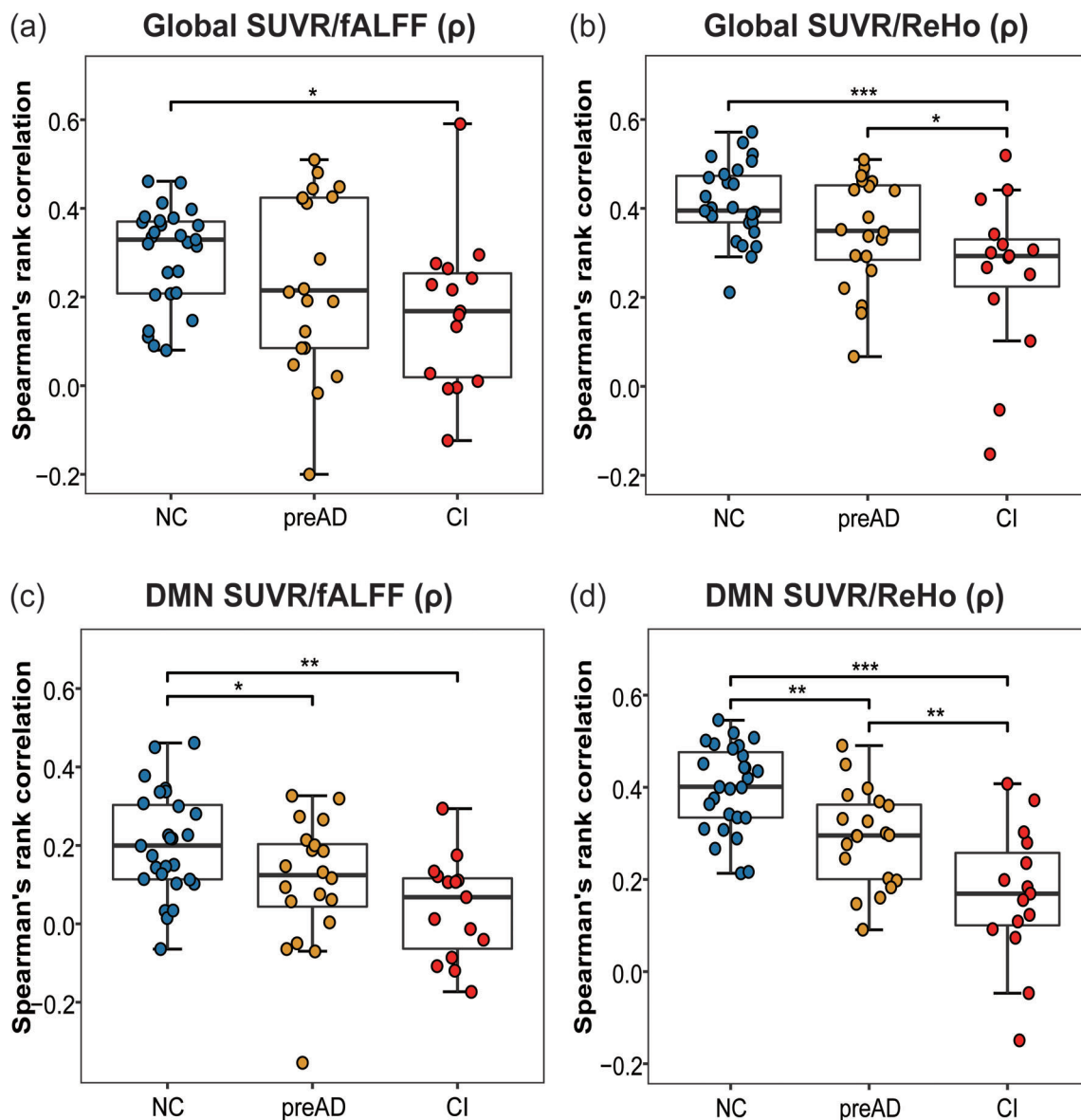
FIGURE 2 Resting-state correlation between FDG SUVR and fMRI indicators within gray matter voxels in individual subjects (all 62). (a) Spearman rank correlation between FDG SUVR and fALFF in normal control (NC), preclinical Alzheimer's disease (preAD), and cognitive impairment (CI) at global brain level, respectively. (b) Same as (a), except that correlation is based on SUVR and ReHo. (c) Same as (a) but at default mode network (DMN) level instead of global brain. (d) Same as (b) but at DMN level instead of entire brain. FDG, fluorodeoxyglucose; fALFF, fractional amplitude of low-frequency fluctuations; ReHo, regional homogeneity; SUVR, standardized uptake value ratio. *$p < .05$, **$p < .01$, ***$p < .001$

(ρ) ($p = .017$, $r = -.348$, Figure 4a), DMNSUVR/fALFF (ρ) ($p < .008$, $r = -.384$, Figure 4b), and DMN SUVR/ReHo (ρ) ($p < .001$, $r = -.584$; Figure 4c) in the cognitive normal subjects. In the entire process of cognitive decline, the significance of this correlation remained stable, and the correlation became more significant with the addition of the CI group (all $p \leq .001$, Figure 4d–f). No correlation was found between the AV45 SUVR and the conventional indicators in normal cognition (all $p > .05$). There was a linear correlation between the AV45 SUVR and the DMN SUVR ($p = .001$, $r = -.453$), DMN fALFF ($p = .009$, $r = -.351$), and DMN ReHo ($p = .004$, $r = -.383$) after the addition of the CI subjects (Figure S2).

3.5 | Classification performance analysis

There were statistically significances in diagnosis of preAD based on the AUC of the ROC curves (Figure 5c) drawn using the DMN SUVR/fALFF (ρ) ($p = .048$, 95% confidence interval (CInt) = [0.515–0.826]) and the DMN SUVR/ReHo (ρ) ($p = .001$, 95% CInt = [0.656–0.980]). However, this was not the case when the conventional indicators were used. Youden's cutoffs of the DMN SUVR/fALFF (ρ) and DMN SUVR/ReHo (ρ) were 1.302 and 1.478, respectively. The sensitivity and specificity of the latter metric were 77.8% and 70.0%, respectively; comparatively, the former had higher
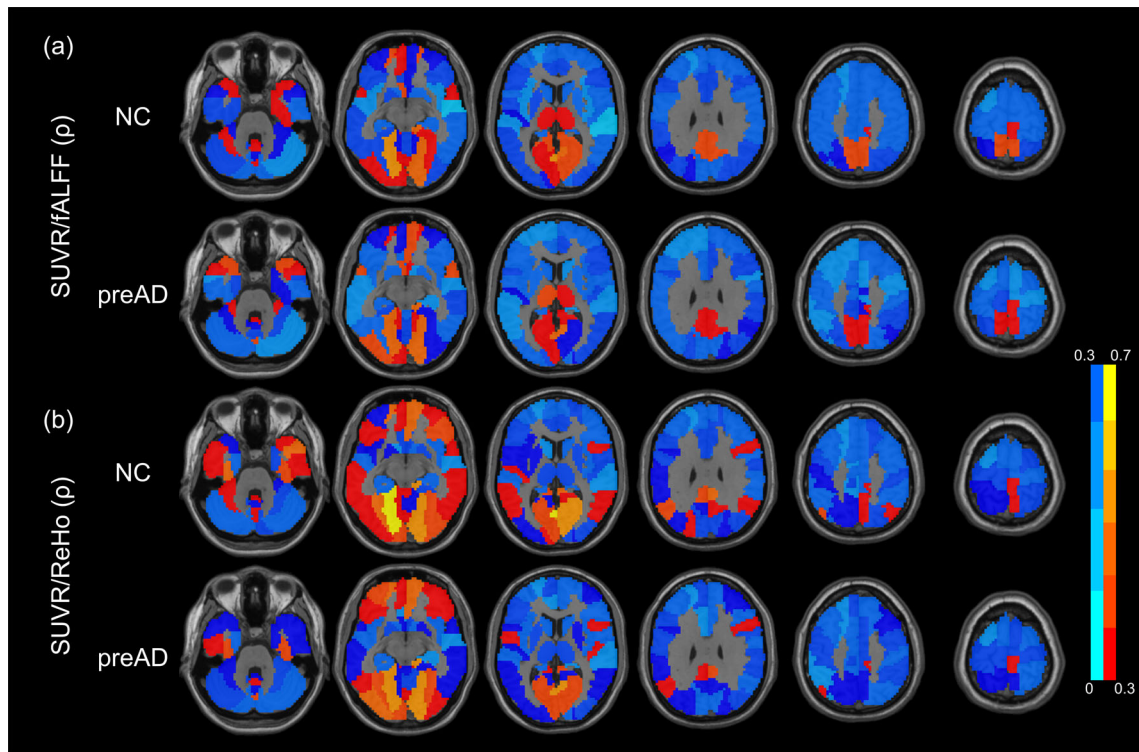
FIGURE 3 Location of high coupling and low coupling regions based on AAL template. The cold color shows low coupling region, and the warm color shows high coupling region. (a) The coupling strength of SUVR/fALFF (ρ) in NC and preAD groups. (b) The coupling strength of SUVR/ReHo (ρ) in NC and preAD groups. AAL, Anatomical Automatic Labeling; fALFF, fractional amplitude of low-frequency fluctuations; NC, normal control; preAD, preclinical Alzheimer's disease; ReHo, regional homogeneity; SUVR, standardized uptake value ratio
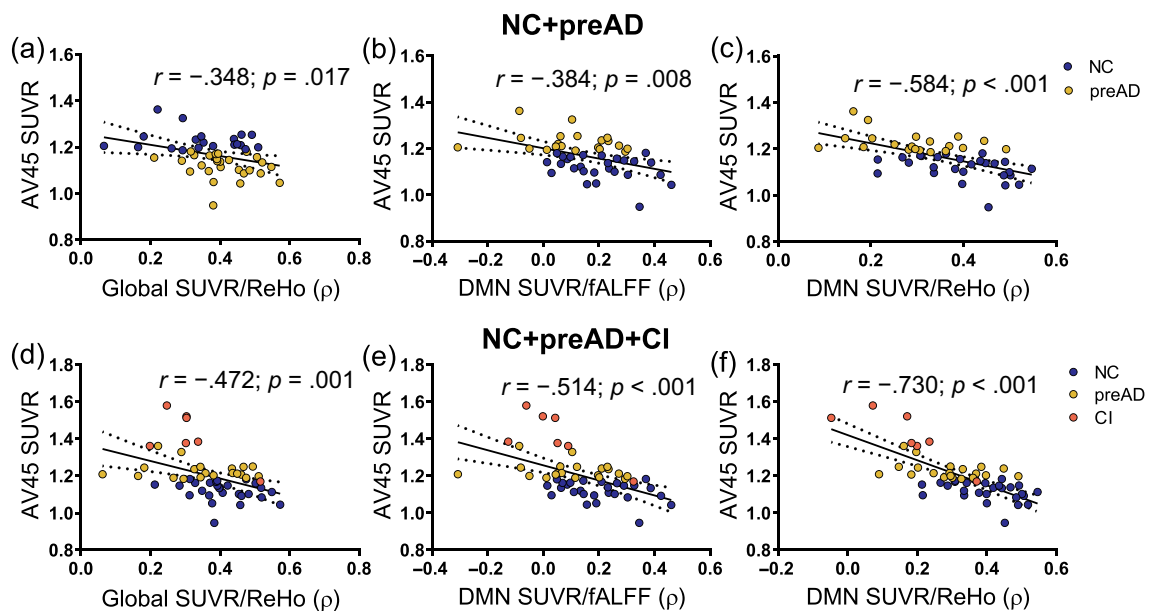
FIGURE 4 Correlation between Amyloid-β (Aβ) and FDG-PET/fMRI correlation metrics. These figures depict partial correlation between FDG-PET/fMRI correlation metrics and AV45 SUVR in cognitively normal and entire disease development population, respectively, which has statistical significance ($p < .05$). (a–c) figures show partial correlation between global SUVR/ReHo (ρ), DMN SUVR/fALFF (ρ), and DMN SUVR/ReHo (ρ) and AV45 SUVR, respectively, in cognitively normal group (NC + preAD). (d–f) figures are same as (a–c) but for entire disease development population (NC + preAD + CI). CI, cognitive impairment; DMN, Default Mode Network; FDG, fluorodeoxyglucose; fALFF, fractional amplitude of low-frequency fluctuations; NC, normal control; preAD, preclinical Alzheimer's disease; ReHo, regional homogeneity; SUVR, standardized uptake value ratio
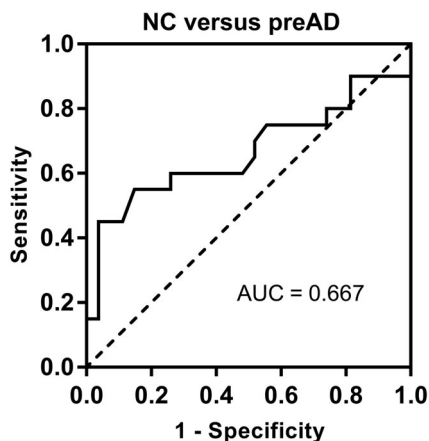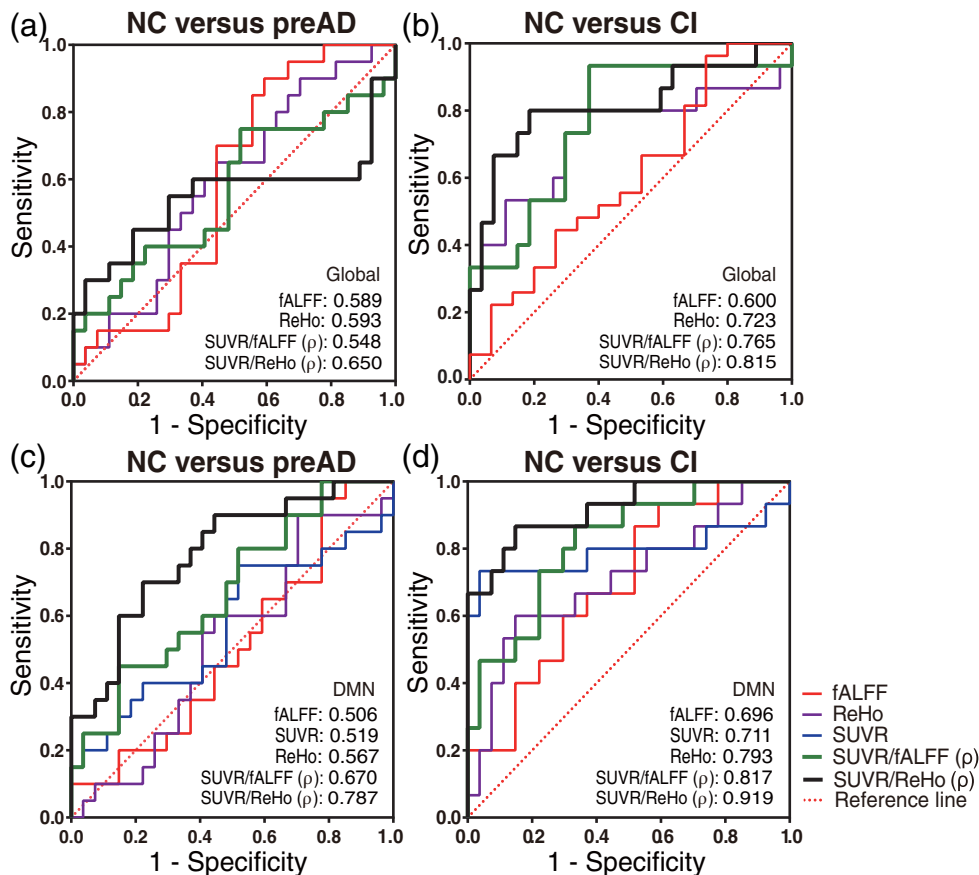
FIGURE 5 Receiver operating characteristic (ROC) curves.
(a) ROC curves of fALFF, ReHo, DMN SUVR/fALFF (ρ) and SUVR/ReHo (ρ) between NC and preAD groups at global brain level.
(b) ROC curves of fALFF, ReHo, DMN SUVR/fALFF (ρ) and SUVR/ReHo (ρ) between NC and CI groups at global brain level.
(c) Same as (a) but at DMN level.
(d) Same as (b) but at DMN level. CI, cognitive impairment; DMN, Default Mode Network; fALFF, fractional amplitude of low-frequency fluctuations; NC, normal control; preAD, preclinical Alzheimer's disease; SUVR, standardized uptake value ratio; ReHo, regional homogeneity

FIGURE 6 Receiver operating characteristic (ROC) curve using lasso for clinical information to distinguish NC and preAD. AUC, area under the curve; NC, normal control; preAD, preclinical Alzheimer's disease

sensitivity (85.2%) but lower specificity (45.0%). Moreover, all the parameters at the entire brain level for the diagnosis of preAD were not very effective (Figure 5a). The results of the AUC analysis of all the indicators for the diagnosis of preAD are summarized in Table S2. The ROC curve of lasso classification of clinical information is shown in Figure 6, and the classification effect is lower than DMN SUVR/ReHo (ρ).

From the ROC analysis of the CI subjects we found that the global SUVR/fALFF (ρ), global SUVR/ReHo (ρ), DMN SUVR/fALFF (ρ), and DMN SUVR/ReHo (ρ) presented excellent diagnostic performance (Figure 5b,d). There AUCs were 0.765 ($p = .005$, 95% CInt = [0.608–0.922]), 0.815 ($p = .001$, 95% CInt = [0.664–0.966]), 0.817 ($p = .001$, 95% CInt = [0.686–0.948]), and 0.919 ($p < .001$, 95% CInt = [0.830–1.000]), respectively. In addition, the conventional indicators (global ReHo, DMN fALFF, and DMN ReHo) also showed good diagnostic performance but lower than the FDG-PET/fMRI correlation metrics (Figure 5c,d). The details are summarized in Table S2. In summary, the FDG-PET/fMRI correlation metrics under the DMN area present better diagnostic performance compared with global level for both preAD and CI, and the performance of the metrics based on ReHo are slightly better than that based on the fALFF.

4 | DISCUSSION

In our study, we used hybrid PET/MRI scanners to evaluate the coupling relationship between glucose consumption assessed via FDG-PET and oxygen metabolism determined by rs-fMRI simultaneously. Importantly, the preAD group was the target group, and we compared the FDG SUVR/ReHo (ρ) and the SUVR/fALFF (ρ) in the NC, preAD, and CI groups in both the global cortex and DMN region. The main findings were as follows:

1. We found that the correlation ρ value of the FDG SUVR/fALFF and the SUVR/ReHo based on DMN region in the preAD stage changed compared to that in the NC subjects. This change was magnified in the CI stage. This suggests that the coupling relationship between the glucose and oxygen metabolisms changes in the early pathogenesis of AD spectrum.

2. Potentially, the FDG SUVR/ReHo (ρ) in the DMN may be a useful biomarker to differentiate NC, preAD, and CI patients.

As shown in Figure 2, CI causes the SUVR/ReHo (ρ) and the SUVR/fALFF (ρ) to significantly weaken compared to those of the NC group at the entire brain level. This is consistent with published studies, proving the reliability of the experimental results and the small impact of PET/MRI scanners (Marchitelli et al., 2018). There is no significant change in preAD at the entire brain level; however, when focusing on the DMN region, preAD significantly weakens the correlation ρ value, which gradually declines during the entire disease. This phenomenon suggests that the change in this coupling relationship starts locally and finally spreads over the entire brain from the pathological level.

As shown in Figure 5, the sensitivity and specificity of the ROC analysis based on the DMN SUVR/ReHo (ρ) for preAD and CI are relatively higher compared to those of the other indicators. Although both the fALFF and ReHo have significant correlations with the FDG SUVR at the individual level, the global or DMN SUVR/ReHo (ρ) is better than the global or DMN SUVR/fALFF. This may be explained as follows: the fALFF is an indicator in the frequency domain. Some scholars believe that in the fALFF method, the grading of the power spectrum causes the power in the low-frequency region (such as the ventricle and sagittal sinus) to be suppressed and change the spectrum distribution (Bu et al., 2019). The fALFF cannot detect subtle information to achieve the best distinction; therefore, even if it is significantly correlated with the FDG SUVR, it may be insufficient to find significant changes in preAD from the perspective of correlation. ReHo reflects the synchronization of the time series of each voxel and its adjacent voxels in the entire brain, which essentially reflects the similarity of the time series between the voxels, instead of the intensity of the activity. It can better reflect the consistency between the voxels and the surrounding voxels, and therefore, is more sensitive to the regulation of neurons and peripheral neurons. The regional regulation of glucose metabolism is consistent with ReHo by the neurovascular regulation, and therefore, the pathological changes of preAD cause abnormal changes in the neurovascular regulation in the brain, which may indirectly have a greater impact on the SUVR/ReHo (ρ) relative to SUVR/fALFF (ρ).

In addition, compared to NC subjects, our study found a decreased glucose metabolism in the angular gyrus, inferior parietal lobule, precuneus, and posterior cingulate cortex in the CI patients. Most of these brain areas are located in the DMN region, which is consistent with previous studies (Gordon et al., 2018; Jack et al., 2017; Landau et al., 2011). Abnormal spontaneous activity in the angular gyrus, right supramarginal cortex, and left middle temporal cortex were found in the resting-state fMRI (Han et al., 2011; Pan

et al., 2017). Our findings are in agreement with those reported by a previous study (Marchitelli et al., 2018). This agreement suggests that our calculated metrics are reliable.

Finally, the SUVR/ReHo (ρ) in the DMN was found to gradually decrease with increasing accumulation of Aβ. The DMN is the most vulnerable network to amyloid deposition (Buckner et al., 2005; Shin et al., 2010; Sperling et al., 2009), showing abnormalities in multiple modalities (Grothe & Teipel, 2016). Precuneus and posterior cingulate cortex, as the key nodes in the DMN, also are highly vulnerable to various pathological changes (Gordon et al., 2018; Malpas et al., 2018), which was further confirmed in this study. Compared with the entire brain level, in the brain region of the DMN, the metabolism, spontaneous activity, and energy–oxygen coupling are related to the global Aβ deposition. The DMN SUVR/ReHo (ρ) is most sensitive to the deposition in the AD progression. As a progressive degenerative entity, the atrophy or metabolic decline of AD is more severe in the late stage of the disease than that in the early stage. Thus, the correlation between the Aβ and the SUVR/fALFF (ρ) or SUVR/ReHo (ρ) became more significant when the CI patients were added to the analytical sample.

Several limitations should be considered. (a) The sample size in this experiment was relatively small. The reliability and repeatability of the coupling relationship should be validated by a relatively larger external multi-center data set. We should notice that the image acquisition scanning protocols differ across different sites. Various fMRI scanning parameters (echo time, voxel size, scan time duration, etc.,) in different sites may result in the inconsistency of fALFF and ReHo (Li, Jin, et al., 2019); and various PET scanning parameters (injected FDG amount, dynamic scan time, etc.,) may also result in the inconsistency of FDG SUVR. Therefore, the deviations may appear when we calculated SUVR/fALFF (ρ) or SUVR/ReHo (ρ) in different sites. It needs to investigate how to reduce the impact of multi-center data in the future. (b) In this exploratory study, we only used the Spearman partial correlation model to express the coupling relationship between the glucose and oxygen metabolisms. Other models may be more practical, which requires more studies in the future. (c) The data used in this study were only cross-sectional, and longitudinal follow-up data need to be further added to validate our experimental results.

5 | CONCLUSION

The coupling relationship between glucose and oxygen metabolisms changed in the preAD stage compared to that in the NC group. The FDG SUVR/ReHo (ρ) in the DMN may be a useful biomarker to differentiate NC, preAD, and CI patients. In addition, this study indicated that hybrid PET/MRI scans are useful in the investigation of the preAD stage.

CONFLICT OF INTEREST

The authors declare no conflict of interest that is directly relevant or directly related to the work described in this manuscript.

ETHICS STATEMENT

The study was approved by the Xuanwu Hospital of Capital Medical University committee and all participants, or their surrogates, gave written informed consent at the time of study enrollment.

PATIENT CONSENT STATEMENT

All the subjects were required to obtain written informed consent prior to enrollment.

PERMISSION TO REPRODUCE MATERIAL FROM OTHER SOURCES

The study did not reproduce material from other sources.

CLINICAL TRIAL REGISTRATION

Experiment name: Prediction of Cognitive Decline by Neuroimaging Techniques and the Application in Diagnosis and Treatment of preclinical AD.

Experiment registration code: NCT03370744.

DATA AVAILABILITY STATEMENT

Some generated or used during the study are proprietary or confidential in nature and may only be provided with restrictions (e.g. original image data). Matlab notebook script are available from the corresponding author upon request.

ORCID

Changchang Ding https://orcid.org/0000-0002-3051-7479
Wenying Du https://orcid.org/0000-0002-3202-5128
Luyao Wang https://orcid.org/0000-0002-9488-4040
Ying Han https://orcid.org/0000-0003-0377-7424
Jiehui Jiang https://orcid.org/0000-0003-4948-3683

REFERENCES

Aiello, M., Salvatore, E., Cachia, A., Pappatà, S., Cavaliere, C., Prinster, A., ... Quarantelli, M. (2015). Relationship between simultaneously acquired resting-state regional cerebral glucose metabolism and functional MRI: A PET/MR hybrid scanner study. *NeuroImage*, 113, 111–121. http://doi.org/10.1016/j.neuroimage.2015.03.017.

Balsis, S., Geraci, L., Benge, J., Lowe, D. A., Choudhury, T. K., Tirso, R., & Doody, R. S. (2018). Statistical model of dynamic markers of the Alzheimer's pathological cascade. *The Journals of Gerontology. Series B, Psychological Sciences and Social Sciences*, 73(6), 964–973. http://doi.org/10.1093/geronb/gbx156.

Baron, J.-C., Rougemont, D., Soussaline, F., Bustany, P., Crouzel, C., Bousser, M., & Comar, D. (1984). Local interrelationships of cerebral oxygen consumption and glucose utilization in normal subjects and in ischemic stroke patients: A positron tomography study. *Journal of Cerebral Blood Flow and Metabolism*, 4, 140–149. http://doi.org/10.1038/jcbfm.1984.22.

Bondi, M. W., Edmonds, E. C., Jak, A. J., Clark, L. R., Delano-Wood, L., McDonald, C. R., ... Salmon, D. P. (2014). Neuropsychological criteria for mild cognitive impairment improves diagnostic precision, biomarker associations, and progression rates. *Journal of Alzheimer's Disease*, 42, 275–289. http://doi.org/10.3233/jad-140276.

Bu, X., Hu, X. Y., Zhang, L. Q., Li, B., Zhou, M., Lu, L., ... Huang, X. Q. (2019). Investigating the predictive value of different resting-state functional MRI parameters in obsessive-compulsive disorder. *Translational Psychiatry*, 9(1), 17. http://doi.org/10.1038/s41398-018-0362-9

Buckner, R. L., Snyder, A. Z., Shannon, B. J., LaRossa, G., Sachs, R., Fotenos, A. F., ... Mintun, M. A. (2005). Molecular, structural, and functional characterization of Alzheimer's disease: Evidence for a relationship between default activity, amyloid, and memory. *The Journal of Neuroscience*, 25, 7709–7717. http://doi.org/10.1523/jneurosci.2177-05.2005.

Chen, K. W., Roontiva, A., Thiyyagura, P., Lee, W., Liu, X. F., Ayutyanont, N., ... Reiman, E. M. (2015). Improved power for characterizing longitudinal amyloid-β PET changes and evaluating amyloid-modifying treatments with a cerebral white matter reference region. *Journal of Nuclear Medicine*, 56(4), 560–566. http://doi.org/10.2967/jnumed.114.149732.

Chételat, G. (2013). Alzheimer disease: Aβ-independent processes-rethinking preclinical AD. *Nature Reviews. Neurology*, 9(3), 123–124. http://doi.org/10.1038/nrneurol.2013.21

Dong, Q. Y., Li, T. R., Jiang, X. Y., Wang, X. N., Han, Y., & Jiang, J. H. (2021). Glucose metabolism in the right middle temporal gyrus could be a potential biomarker for subjective cognitive decline: A study of a Han population. *Alzheimer's Research & Therapy*, 13(1), 74. http://doi.org/10.1186/s13195-021-00811-w.

Duan, H. Q., Jiang, J. H., Xu, J., Zhou, H. C., Huang, Z. M., Yu, Z. H., & Yan, Z. Z. (2016). Differences in Aβ brain networks in Alzheimer's disease and healthy controls. *Brain Research*, 1655, 77–89. https://doi.org/10.1016/j.brainres.2016.11.019.

Dubois, B., Feldman, H. H., Jacova, C., Hampel, H., Molinuevo, J. L., Blennow, K., ... Cummings, J. L. (2014). Advancing research diagnostic criteria for Alzheimer's disease: The IWG-2 criteria. *Lancet Neurology* 13(6), 614–629. https://doi.org/10.1016/s1474-4422(14)70090-0

Folstein, M. F., Folstein, S. E., & McHugh, P. R. (1975). "Mini-mental state". *Journal of Psychiatric Research*, 12(3), 189–198. http://doi.org/10.1016/0022-3956(75)90026-6.

Gonzalez-Escamilla, G., Lange, C., Teipel, S., Buchert, R., Grothe, M. J. (2017). PETPVE12: an SPM toolbox for Partial Volume Effects correction in brain PET – Application to amyloid imaging with AV45-PET. *NeuroImage*, 147, 669–677. http://doi.org/10.1016/j.neuroimage.2016.12.077.

Gordon, B. A., Blazey, T. M., Su, Y., Hari-Raj, A., Dincer, A., Flores, S., ... Benzinger, T. L. S. (2018). Spatial patterns of neuroimaging biomarker change in individuals from families with autosomal dominant Alzheimer's disease: A longitudinal study. *Lancet Neurology*, 17(3), 241–250. http://doi.org/10.1016/s1474-4422(18)30028-0.

Grothe, M. J., & Teipel, S. J. (2016). Spatial patterns of atrophy, hypometabolism, and amyloid deposition in Alzheimer's disease correspond to dissociable functional brain networks. *Human Brain Mapping*, 37(1), 35–53. http://doi.org/10.1002/hbm.23018.

Gupta, V. (2020): Reader response: Neuropathological features associated with basal forebrain atrophy in Alzheimer's disease.

Habib, M., Mak, E., Gabel, S., Su, L., Williams, G., Waldman, A., ... O'Brien, J. T. (2017). Functional neuroimaging findings in healthy middle-aged adults at risk of Alzheimer's disease. *Ageing Research Reviews*, 36, 88–104. http://doi.org/10.1016/j.arr.2017.03.004.

Han, Y., Wang, J., Zhao, Z., Min, B., Lu, J., Li, K., ... Jia, J. (2011). Frequency-dependent changes in the amplitude of low-frequency fluctuations in amnestic mild cognitive impairment: A resting-state fMRI study. *NeuroImage*, 55(1), 287–295. https://doi.org/10.1016/j.neuroimage.2010.11.059.

Jack, C. R. J., Wiste, H. J., Weigand, S. D., Therneau, T. M., Lowe, V. J., Knopman, D. S., ... Petersen, R. C. (2017). Defining imaging biomarker cut points for brain aging and Alzheimer's disease. *Alzheimers Dement*, 13(3), 205–216. http://doi.org/10.1016/j.jalz.2016.08.005.

Jessen, F., Amariglio, R. E., Buckley, R. F., van der Flier, W. M., Han, Y., Molinuevo, J. L., ... Wagner, M. (2020). The characterisation of subjective cognitive decline. *Lancet Neurology*, 19(3), 271–278. http://doi.org/10.1016/s1474-4422(19)30368-0.

Jueptner, M., & Weiller, C. (1995). Review: Does measurement of regional cerebral blood flow reflect synaptic activity?—Implications for PET and fMRI. *NeuroImage*, 2(2), 148–156. http://doi.org/10.1006/nimg.1995.1017.

Landau, S. M., Harvey, D., Madison, C. M., Koeppe, R. A., Reiman, E. M., Foster, N. L., ... Jagust, W. J. (2011). Associations between cognitive, functional, and FDG-PET measures of decline in AD and MCI. *Neurobiology of Aging*, 32(7), 1207–1218. http://doi.org/10.1016/j.neurobiolaging.2009.07.002.

Li, J. C., Jin, D., Li, A., Liu, B., Song, C. Y., Wang, P., ... Han, Y. (2019). ASAF: Altered spontaneous activity fingerprinting in Alzheimer's disease based on multisite fMRI. *Scientific Bulletin*, 64(14), 998–1010. http://doi.org/10.1016/j.scib.2019.04.034

Li, X. Y., Wang, X. N., Su, L, Hu, X. C., & Han, Y. (2019). Sino longitudinal study on cognitive decline (SILCODE): Protocol for a Chinese longitudinal observational study to develop risk prediction models of conversion to mild cognitive impairment in individuals with subjective cognitive decline. *BMJ Open*, 9(7), e028188. http://bmjopen.bmj.com/content/9/7/e028188.abstract

Malpas, C. B., Saling, M. M., Velakoulis, D., Desmond, P., Hicks, R. J., Zetterberg, H., ... O'Brien, T. J. (2018). Cerebrospinal fluid biomarkers are differentially related to structural and functional changes in dementia of the Alzheimer's type. *Journal of Alzheimer's Disease*, 62(1), 417–427. http://doi.org/10.3233/jad-170250.

Marchitelli, R., Aiello, M., Cachia, A., Quarantelli, M., Cavaliere, C., Postiglione, A., ... Pappatà, S. (2018). Simultaneous resting-state FDG-PET/fMRI in Alzheimer disease: Relationship between glucose metabolism and intrinsic activity. *NeuroImage*, 176, 246–258. http://doi.org/10.1016/j.neuroimage.2018.04.048.

McKhann, G. M., Knopman, D. S., Chertkow, H., Hyman, B. T., Jack, C. R., Kawas, C. H., ... Phelps, C. H. (2011). The diagnosis of dementia due to Alzheimer's disease: Recommendations from the National Institute on Aging-Alzheimer's Association workgroups on diagnostic guidelines for Alzheimer's disease. *Alzheimer's & Dementia*, 7(3), 263–269. http://doi.org/10.1016/j.jalz.2011.03.005

Molinuevo, J. L., Rabin, L. A., Amariglio, R., Buckley, R., Dubois, B., Ellis, K. A., ... Jessen, F. (2017). Implementation of subjective cognitive decline criteria in research studies. *Alzheimer's & Dementia*, 13(3), 296–311. http://doi.org/10.1016/j.jalz.2016.09.012.

Mukaka, M. M. (2012). Statistics corner: A guide to appropriate use of correlation coefficient in medical research. *Malawi Medical Journal*, 24(3), 69–71. Retrieved from http://pubmed.ncbi.nlm.nih.gov/23638278

Palaniyappan, L., & Liddle, P. F. (2014). Diagnostic discontinuity in psychosis: A combined study of cortical gyrification and functional connectivity. *Schizophrenia Bulletin*, 40(3), 675–684. https://doi.org/10.1093/schbul/sbt050.

Pan, P. L., Zhu, L., Yu, T. T., Shi, H. C., Zhang, B., Qin, R. M., ... Xu, Y. (2017). Aberrant spontaneous low-frequency brain activity in amnestic mild cognitive impairment: A meta-analysis of resting-state fMRI studies. *Ageing Research Reviews*, 35, 12–21. http://doi.org/10.1016/j.arr.2016.12.001.

Pegueroles, J., Vilaplana, E., Montal, V., Sampedro, F., Alcolea, D., Carmona-Iragui, M., ... Fortea, J. (2017). Longitudinal brain structural changes in preclinical Alzheimer's disease. *Alzheimer's & Dementia*, 13(5), 499–509. http://doi.org/10.1016/j.jalz.2016.08.010.

Shin, J., Lee, S.-Y., Kim, S. J., Kim, S.-H., Cho, S.-J., & Kim, Y.-B. (2010). Voxel-based analysis of Alzheimer's disease PET imaging using a triplet of radiotracers: PIB, FDDNP, and FDG. *NeuroImage*, 52(2), 488–496. http://doi.org/10.1016/j.neuroimage.2010.04.013.

Sperling, R. A., Aisen, P. S., Beckett, L. A., Bennett, D. A., Craft, S., Fagan, A. M., ... Phelps, C. H. (2011). Toward defining the preclinical stages of Alzheimer's disease: Recommendations from the National Institute on Aging-Alzheimer's Association workgroups on diagnostic guidelines for Alzheimer's disease. *Alzheimer's & Dementia*, 7(3), 280–292. http://doi.org/10.1016/j.jalz.2011.03.003

Sperling, R. A., Laviolette, P. S., O'Keefe, K., O'Brien, J., Rentz, D. M., Pihlajamaki, M., ... Johnson, K. A. (2009). Amyloid deposition is associated with impaired default network function in older persons without dementia. *Neuron*, 63(3), 178–188. http://doi.org/10.1016/j.neuron.2009.07.003.

Sun, Y., Dai, Z., Li, Y., Sheng, C., Li, H., Wang, X., ... Han, Y. (2016). Subjective cognitive decline: Mapping functional and structural brain changes-a combined resting-state functional and structural MR imaging study. *Radiology*, 281(1), 185–192. http://doi.org/10.1148/radiol.2016151771.

Wang, M., Jiang, J. H., Yan, Z. Z., Alberts, I., Ge, J. J., Zhang, H. W., ... Shi, K. Y. (2020). Individual brain metabolic connectome indicator based on Kullback-Leibler divergence similarity estimation predicts progression from mild cognitive impairment to Alzheimer's dementia. *European Journal of Nuclear Medicine and Molecular Imaging*, 47(12), 2753–2764. http://doi.org/10.1007/s00259-020-04814-x

Wang, X. Q., Huang, W. J., Su, L., Xing, Y., Jessen, F., Sun, Y., ... Han, Y. (2020). Neuroimaging advances regarding subjective cognitive decline in preclinical Alzheimer's disease. *Molecular Neurodegeneration*, 15(1), 55. http://doi.org/10.1186/s13024-020-00395-3

Xie, C., Bai, F., Yuan, B., Yu, H., Shi, Y., Yuan, Y., ... Zhang, Z.-J. (2015). Joint effects of gray matter atrophy and altered functional connectivity on cognitive deficits in amnestic mild cognitive impairment patients. *Psychological Medicine*, 45(9), 1799–1810. http://doi.org/10.1017/s0033291714002876.

Yan, S. Z., Zheng, C. J., Cui, B. X., Qi, Z. G., Zhao, Z. L., An, Y. H., ... Lu, J. (2020). Multiparametric imaging hippocampal neurodegeneration and functional connectivity with simultaneous PET/MRI in Alzheimer's disease. *European Journal of Nuclear Medicine and Molecular Imaging*, 47(10), 2440–2452. http://dx.doi.org/10.1007/s00259-020-04752-8

Yeo, B. T. T., Krienen, F. M., Sepulcre, J., Sabuncu, M. R., Lashkari, D., Hollinshead, M., ... Buckner, R. L. (2011). The organization of the human cerebral cortex estimated by intrinsic functional connectivity. *Journal of Neurophysiology*, 106(3), 1125–1165. http://doi.org/10.1152/jn.00338.2011.

Zang, Y. F., Jiang, T. Z., Lu, Y. L., He, Y., & Tian, L. X. (2004). Regional homogeneity approach to fMRI data analysis. *NeuroImage*, 22(1), 394–400. http://doi.org/10.1016/j.neuroimage.2003.12.030.

Zou, Q. H., Zhu, C. Z., Yang, Y. H, Zuo, X. N., Long, X. Y., Cao, Q. J., ... Zang, Y. F. (2008). An improved approach to detection of amplitude of low-frequency fluctuation (ALFF) for resting-state fMRI: Fractional ALFF. *Journal of Neuroscience Methods*, 172(1), 137–141. http://doi.org/10.1016/j.jneumeth.2008.04.012.

Zuo, X. N., Di Martino, A., Kelly, C., Shehzad, Z. E., Gee, D. G., Klein, D. F., ... Milham, M. P. (2010). The oscillating brain: Complex and reliable. *NeuroImage*, 49(2), 1432–1445. http://doi.org/10.1016/j.neuroimage.2009.09.037.

SUPPORTING INFORMATION

Additional supporting information may be found online in the Supporting Information section at the end of this article.